Codebook Design for Holographic MIMO: Near-Field Prospects and Road to Standardization

Yuanbin Chen[1], Dongxuan He[2], Shunyu Li[3], Tianqi Mao[3,4,*]

[1]School of Electrical and Electronic Engineering, Nanyang Technological University, Singapore 639798
[2]School of Information and Electronics, Beijing Institute of Technology, Beijing 100081, China
[3]State Key Laboratory of CNS/ATM, Beijing Institute of Technology, Beijing 100081, China
[4]MIIT Key Laboratory of Complex-Field Intelligent Sensing, Beijing Institute of Technology, Beijing 100081, China
([*]Corresponding author; Email: maotq@bit.edu.cn)

2025 International Wireless Communications and Mobile Computing (IWCMC) | 979-8-3315-0887-6/25/$31.00 ©2025 IEEE | DOI: 10.1109/IWCMC65282.2025.11059433

***Abstract*—Holographic multiple-input multiple-output (HMIMO) is envisaged as a viable manner for manipulating electromagnetic field produced or perceived by antennas, in an effort to achieve an intelligent and endogenously holography-capable wireless propagation environment. This notion garners significant interest when engaging large antenna elements at high frequencies, such as millimeter-wave or terahertz. Under these conditions, operations often occur within the Fresnel region, i.e., near-field region, where assumptions of planar wavefront no longer apply. This article investigates the codebook solution for HMIMO, unmasking a number of challenges intrinsic in the near-field context and limitations of applying codebooks specified in current standards. Specifically, we proposed a two-phase codebook design empowered by artificial intelligence (AI)-based techniques, where angular and distance ingredients are resolved respectively at each phase, functioning in tandem for facilitating an efficient beam training at reduced pilot overhead. Then from the 3rd generation partnership project (3GPP) standardization perspective, we share potential design rationales influencing standardization, along with a novel signaling procedure for HMIMO beam sweeping.**

***Index Terms*—Holographic MIMO, 6G, near-field communications, codebook design, standardization.**

I. Introduction

The fifth-generation (5G) base stations (BSs) with massive multiple-input multiple-output (mMIMO) capabilities have marked their successful commercial footprints across diverse nations and regions. Amidst the unending saga of such technological evolution, the wireless communications community remains unwavering in its commitment to exploring and sculpting future MIMO technologies with qualities hitherto unimagined - extremely high spectral and energy efficiency, ultra-low latency, and seamless connectivity. In this pursuit, it is anticipated to leverage antenna densification and large antenna arrays in future sixth-generation (6G) communications [1]. In the presence of classical operating conditions (that is, within the Fraunhofer region of the antenna), the distance of the communication link far exceeds the size of antenna aperture, so the planar-wavefront propagation is typically assumed. However, this case takes an intriguing turn when the communication link shifts into the Fresnel region characterized by the near-field propagation [2]. For instance, in the case where antennas, with their aperture sizes extending from 10 cm to 1 m, are employed over the mmWave frequency band, the typical operating distances encircling around a hundred meters are almost entirely enveloped within the Fresnel region. This invalidates the planar-wavefront assumption, and a spherical-wavefront case must be considered instead. Therefore, the operation occurring below the boundary of the Fraunhofer region necessitates the examination of novel models embracing this regime, which, in turn, paves the way for uncharted possibilities to boost the performance of communication systems.

To fully harness the attributes of electromagnetic (EM) propagation mechanisms and hence edge ever closer to the limits of wireless channels, a holistic control of the EM fields sensed/generated by antennas should be realized, which conceptualizes the essence of the *holographic communication*. Viewed through its physical fundamentals, the advancement in meta-materials provides a viable solution for realizing highly flexible antenna elements, allowing the manipulation of the EM field and the precise control of amplitude and phase at an unprecedented level. To abstract from the specific implementations of meta-materials, the meta-surface can be modeled as a continuous array consisting of infinitesimally small antenna elements (i.e., a nearly continuous aperture). Wireless communication utilizing innumerable antenna elements within a finite spatial expanse has been coined as *holographic MIMO (HMIMO)* [3]–[6]. With the theoretical integration of numerous antenna elements in a continuous aperture, one can treat this as the asymptotic limit of mMIMO. However, the increasing size of the surfaces poses a challenge, i.e., wireless propagation at mmWave of terahertz frequencies may transpire within the near-field region of the antenna. Thus, the planar-wavefront assumptions cease to retain their validity.

Fully unleashing the potential of HMIMO in the near-field context relies upon the efficient acquisition of channel state information (CSI). The techniques of CSI acquisition in MIMO systems can be informally classified into two categories: explicit CSI acquisition, which signifies channel estimation, and implicit

CSI acquisition, a term synonymous with beam training. Although explicit CSI acquisition can precisely identify channel parameters, the surge in overhead scaling with an increasing number of antenna elements poses significant challenges for implementations of HMIMO. In contrast, beam training aims to detect the physical directions of channel paths, rather than the entire channel. In comparison to explicit channel estimation, beam training is capable of directly establishing reliable beamforming via the beam sweeping, circumventing the unfavorable estimation that often occurs under poor signal-to-noise ratio (SNR) conditions at the receiver. Hence, beam training enjoys wide implementation in current 5G MIMO systems, namely 5G new radio (NR) Type I and Type II codebooks specified in Release 17 TS 38.214 [7]. Regardless of the CSI acquisition considered, the near-field context entails additional distance information compared to the far-field counterpart, primarily due to the characteristics inherent in spherical-wavefront model.

At present, a few fledgling initiatives have investigated CSI acquisition for HMIMO regime and its relatives, such as extremely-large MIMO (XL-MIMO), with the main efforts focusing on near-field channel estimation [2], [8] and near-field beam training [9]. Among these impressive efforts, different approaches have been adopted to achieve favorable performance, using techniques drawn from compressive sensing (CS)-based techniques [2], [8], and deep learning [9]. However, there remains an absence in thoroughly investigating the holographic characteristics and envisioning their future standardization possibilities thus far. Specifically, the questions listed below have not been adequately answered:

Q1: How does near-field codebook design differ in HMIMO regime compared to that in the conventional MIMO?

Q2: In the presence of novel characteristics, how to design near-field holographic codebook while taking into account practical complexity and signaling overhead?

Q3: How far should we go, based on the current standardization process of 3GPP AI-enabled air interface, to standardize the HMIMO codebook empowered by AI?

Geared towards three questions outlined, the current work set out with the aim of filling the knowledge gap in the state-of-the-art by following contributions:

- We present several peculiarities inherent in near-field HMIMO systems, primarily by shedding light on the limitations of applying far-field codebooks, as are currently utilized in 5G NR, for near-field beam training in holographic contexts (for Q1).
- Inspired by artificial intelligence (AI)-based approach, a two-phase procedure is proposed aimed at tackling the angular and distance ingredients of near-field HMIMO systems, facilitating the efficient beam training at reduced pilot overhead (for Q2).
- To be forward compatible with existing codebooks in 5G NR standard, based on the state-of-the-art in AI-enabled air interface, we envision the potential design rationales influencing standardization, along with a novel two-phase signaling procedure for HMIMO beam sweeping (for Q3).

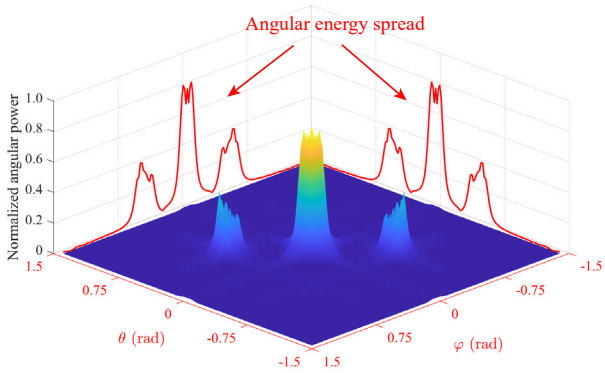

(a) Angular energy spread

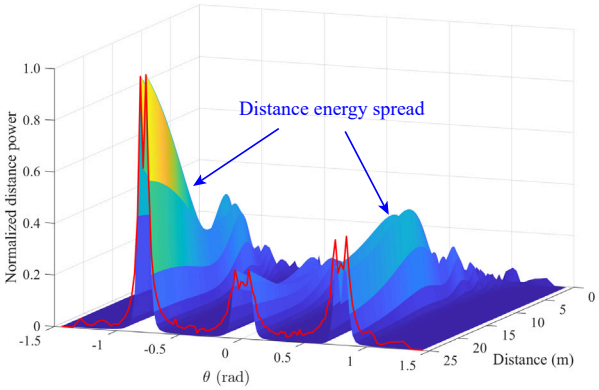

(b) Distance energy spread

Fig. 1. Illustration of near-field energy spread. We assume there are three scatterers in the propagation environment.

II. Peculiarities of Near-Field HMIMO Regimes

The leap from mMIMO to HMIMO covers more than a simple change in antenna array morphology, such as more densely packed antenna elements, increased number of antenna elements, and increased size of array, entailing a fundamental shift in the structure of the EM propagation field. To glean deeper insights, we commence by examining several peculiarities of near-field HMIMO systems, including its intrinsic properties and potential ramifications. These explorations are essential in streamlining practical implementation and facilitating performance evaluation.

A. Spatial Non-Stationarity of Holographic Array

As the number of holographic antenna elements increases, it is observed that signals arrive with varying angles of arrival (AoAs) at different elements. This indicates different parts of the array may sense the same channel paths with varied powers or observe different paths altogether [8], [10]. The conventional belief that each element shares a common AoA for the same

path is no longer valid. In traditional array modeling, which treats each element as a sizeless point, the effective apertures of these elements might vary significantly. Failing to account for this variation may result in the received power exceeding the transmit power as the array size grows, a phenomenon termed as *spatial non-stationarity* [11].

The spatial non-stationarity tends to appear across the holographic array, imposing a departure from the commonly used channel model. A cluster-based geometric channel model reflects more appropriately the cause of non-stationarity, with the expression of steering vectors being the major change in comparison to their traditional models. Particularly, the phase of each entry should be modeled using spherical waves in the vicinity of the array, since the planar wave approximation is no longer viable. Secondly, the amplitude of each element fluctuates. This is attributed to the path loss along the array as well as to the interactions between clusters and blocks in the environment, because various segments of the spherical wavefront experience different propagation characteristics.

B. Near-Field Energy Spread

The way to separate radiative near-field versus far-field regions is the classical Rayleigh distance $r_{\text{Rayl}} = 2D^2/\lambda$, with D and λ representing the physical size of antenna aperture and signal wavelength, respectively. With regard to mMIMO systems, the Rayleigh distance spans only a trivial few meters, resulting in the design of existing Type I and Type II codebooks being based on far-field planar-wavefront models. However, when evolving to the HMIMO regime, the considerable increase in the number of antenna elements pushes the Rayleigh distance to a dimension that can no longer be disregarded – potentially expanding to hundreds of meters. This implies that scattering is more likely to occur in the near-field region.

However, the implementation of beam training in the near-field region employing Type I and Type II codebooks, which only covers the angular information lopsidedly, may lead to the energy spread. For simplicity, we herein follow the philosophy of Type I codebook to examine this issue. Fig. 1 portrays the power scattered in relation to the azimuth-elevation angle pair (θ, φ) in Fig. 1(a) and the distance in Fig. 1(b), respectively. It is assumed that there are three scatterers in the propagation environment. As transpired in Fig. 1(a), the normalized angular power scattered typically results in the proliferation of angles, and fluctuates rapidly across the holographic antenna array. Despite the detachment of distance, the true azimuth-elevation angle pair (θ, φ) cannot be precisely distinguished, as opposed to being concentrated on a few single peaks in the far-field region. Furthermore, as illustrated in Fig. 1(b), the power scattered versus the distance reveals a fluctuating trend from peak to trough. In this case, it is difficult to distinguish the genuine scattered power of the exact significant distance, since the energy may spread farther away with increased distance.

C. Potential Overhead

The incorporation of additional distance ingredient inevitably results in an increase in the pilot overhead when customizing novel codebook for HMIMO systems. The overhead is typically considered as the resource element (RE) that is occupied by the uplink pilot sent to the BS over an orthogonal frequency division multiplexing (OFDM) symbol. On the one hand, with an increase in the number of antenna elements, there is a need to configure additional directions for beam sweeping, resulting in the occupation of more time slots. On the other hand, in the near-field environment, once the user equipment (UE) delivers feedback of the exact beam direction to the BS, the distance sweeping has to be further carried out to determine the significant distance. This requires additional pilot procedure for identifying significant distances.

III. AI-Enabled Two-Phase Holographic Codebook Solution

In this section, we devise a two-phase holographic codebook, in an attempt to adjust the codebook size for striking beneficial tradeoffs between the sampling complexity, pilot overhead, and the beam training performance. This design indeed poses an arduous task, primarily due to i) the implicit angle-distance coherence and ii) the limited information that can be extracted from the received signal. This renders conventional channel estimation techniques in excessively complex. To tackle these challenges, we leverage AI-based techniques, which exhibit strong abilities in acquiring intricate non-linear relationships, to facilitate the holographic codebook design [12].

As illustrated in Fig. 2, the considered holographic metasurface is a uniform planar array (UPA) having $N = N_y \times N_z$ antenna elements. The Cartesian coordinate system is adopted, where the $y-z$ plane coincides with the UPA, the $x-$axis is vertical to the UPA, and the origin is located at the center of the UPA. N_{RF} feeds are uniformly spaced on the surface of the UPA, with each attached to a radio frequency (RF) chain. The number of antenna elements along the $y-$axis and $z-$axis is N_y and N_z, respectively. Without loss of generality, we denote (n_y, n_z) by the index of an arbitrary antenna element positioned on the surface of UPA. The proposed holographic codebook solution consists of two phases, each aimed at determining significant angles and distances, as detailed below.

A. Phase I

In Phase I, UE sends P pilots to the BS, and the received uplink signal at the BS is given by $\mathbf{y}^{\text{I}} \in \mathbb{C}^{PN_{\text{RF}} \times 1}$, in which P pilots determines PN_{RF} angular samples. These angular samples serve as the inputs to the AI network for feature extraction. In this phase, an angular-wise codebook composed of significant angle information is drawn from $\mathbf{y}^{\text{I}}$. Furthermore, convolution neural network (CNN) is employed to implement the recovery of the angular codebook owing to its robust performance in classification tasks [12]. The proposed CNN-based model is portrayed in Fig. 3(a), consisting of three

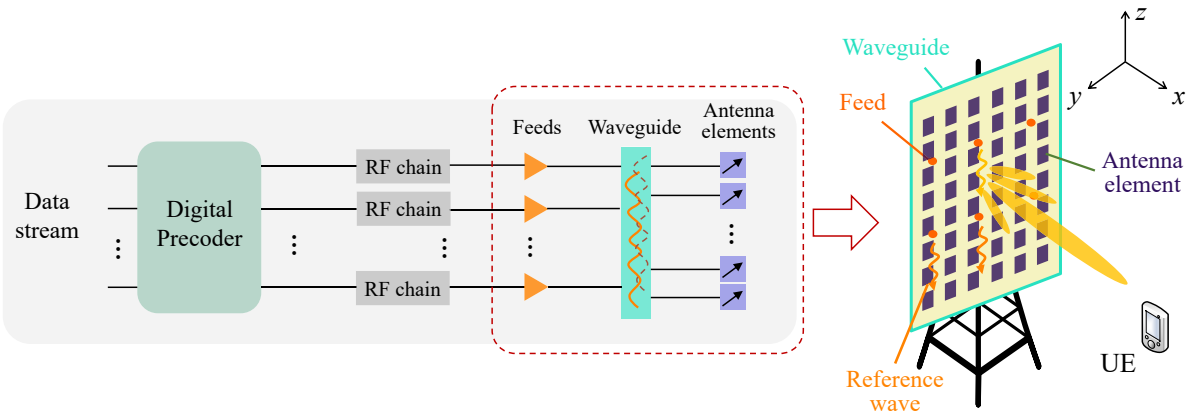

Fig. 2. A framework of the HMIMO system, where the holographic meta-surface is a UPA having $N = N_y \times N_z$ antenna elements. N_{RF} feeds are embedded in the substrate (waveguide) in order to generate reference waves carrying user-intended signals, with each feed connected to a radio frequency (RF) chain for signal processing.

entities, i.e., the preprocessing entity, the convolution entity, and the output entity, which are elaborated as follows.

1) Preprocessing Entity: Given that the received signal $\mathbf{y}^{\text{I}}$ is typically complex-valued with uncertain fluctuations and thus cannot be fed directly to CNN, $\mathbf{y}^{\text{I}}$ is first normalized using its maximum amplitude of its entiries. Then, the obtained normalized signal $\mathbf{y}^{\text{I}}_{\text{Norm}}$ is divided into a pair of real-valued quantities, which are fed to the subsequent convolution entity.

2) Convolution Entity: The hidden features of $\mathbf{y}^{\text{I}}_{\text{Norm}}$ are extracted using multiple convolution layers, with each convolution layer followed by a rectified linear unit (ReLU) activation layer to provide nonlinear adaptability. After the final ReLU activation layer, a pooling layer is introduced for avoiding the overwhelming complex model. In this case, each real-valued quantity is downsampled to be a scalar. Furthermore, the cross entropy loss is selected as the evaluation metric for classification tasks during the training procedure.

3) Output Entity: Upon completion of the pooling layer, the full-connected (FC) layer is incorporated to transform the extracted features to the candidate indices of significant angles. Subsequently, using a softmax activation layer, the output returns to a probability vector, i.e., $\hat{\boldsymbol{p}}^{\text{I}} = \left[\hat{p}^{\text{I}}_1, ..., \hat{p}^{\text{I}}_N\right] \in \mathbb{C}^{N\times 1}$, where $\hat{p}^{\text{I}}_n$ is the predicted probability for the nth angular sample. Thus, the optimal index associated with the significant angle can be determined by the maximum predicted probability, i.e., $\hat{n}^* = \arg\max_{n\in\{1,2,...,N\}} \hat{p}^{\text{I}}_n$. Eventually, a total of $\tilde{N}$ probabilities will be picked, implying that only $\tilde{N}$ codewords corresponding to these $\tilde{N}$ significant angles are required to construct the angular-wise codebook. Furthermore, the obtained probability vector in Phase I serves as the input for the subsequent phase, implying that the distance sweeping is based on $\tilde{N}$ significant angles determined.

B. Phase II

Having obtained the optimal angular index associated with significant angles, the distance sweeping is carried out in this phase. Fig. 3(b) illustrates that the inputs of Phase II consist of the probability vector $\hat{\boldsymbol{p}}^{\text{I}}$ from Phase I and the signal $\mathbf{y}^{\text{II}}$ received after the UE transmits S pilots. Each entry in $\mathbf{y}^{\text{II}}$ achieves the incoherence angular-distance sampling for determining significant distances using SN_{RF} samples. Given the heterogeneity of this pair of inputs, we employ an attention-based model, as depicted in Fig. 3(b), which effectively fuses features from both phases. This model can adaptively weigh features in the fused vector $\left[\hat{\boldsymbol{p}}^{\text{I}}; \mathbf{y}^{\text{II}}\right]$, allowing the model itself to prioritize more important features.

After the attention entity, the CNN employed for identifying significant distances resembles that in Phase I, including the preprocessing entity, the convolution entity, and the output entity, as showcased in Fig. 3(b). Likewise, the output returns to a probability vector $\hat{\boldsymbol{p}}^{\text{II}} = \left[\hat{p}^{\text{II}}_1, ..., \hat{p}^{\text{II}}_U\right] \in \mathbb{C}^{U\times 1}$, where $\hat{p}^{\text{II}}_u$ is the predicted probability for the uth distance sample among U distance samples in total. Then, the optimal index associated with the significant distance can be identified by the maximum predicted probability, i.e., $\hat{u}^* = \arg\max_{u\in\{1,2,...,U\}} \hat{p}^{\text{II}}_u$. Accordingly, a total of $\tilde{U}$ probabilities are picked out, for establishing distance-wise codebook comprised of $\tilde{U}$ codewords corresponding to these $\tilde{U}$ significant distances.

In order to evaluate the performance of the proposed AI-enabled two-phase codebook scheme, Fig. 4 depicts the achievable rate as a function of the BS-UE distance for various benchmarks. Particularly, the benchmark schemes employed are given as follows. i) Perfect CSI: the holographic codebook is generated via meticulous, fine-grained sampling across both the angular and distance domains. ii) Conventional scheme: this scheme takes its cue from the basic idea underlying Type I and Type II codebooks, e.g., uniform angular and distance sampling, to generate holographic codebook. As tran-

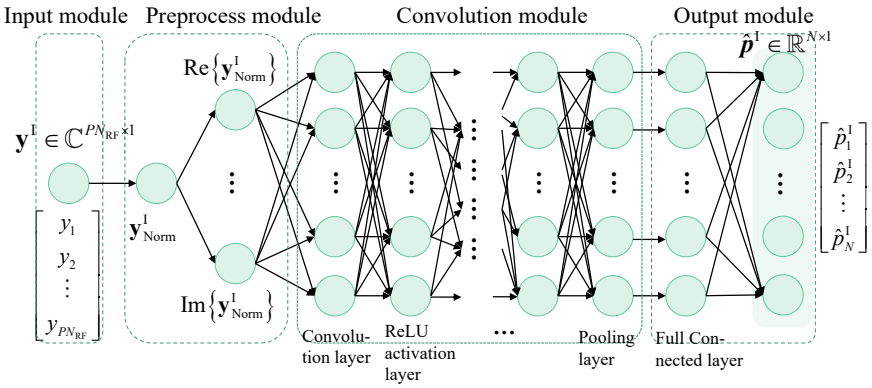

(a) Phase I

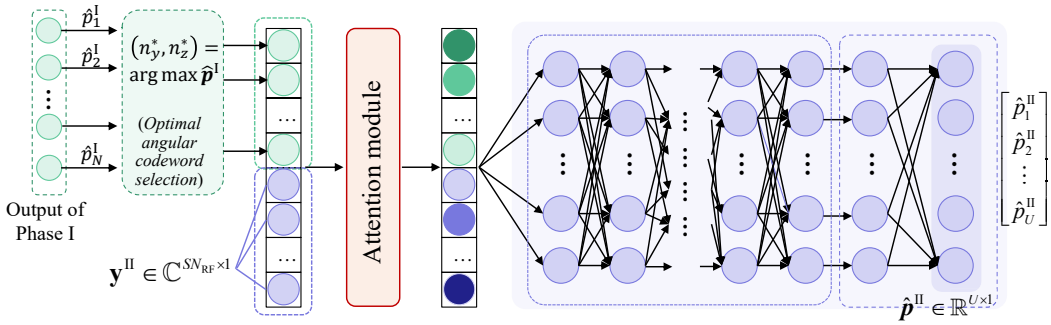

(b) Phase II

Fig. 3. The proposed AI-enabled two-phase holographic codebook solution.

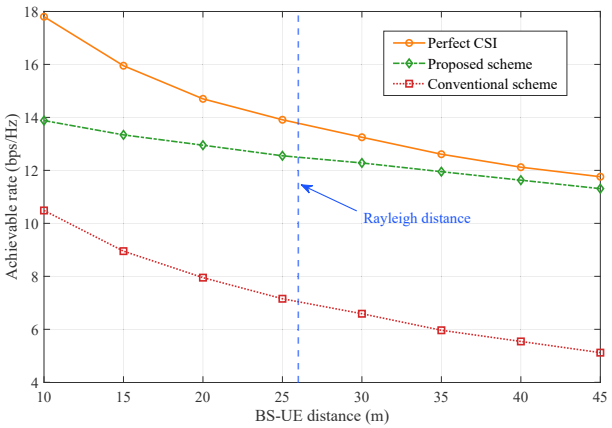

Fig. 4. Achievable rate versus BS-UE distance. The number of antenna elements is configured as $N_y = 129$, $N_z = 65$, and the considered HMIMO system operates at 30 GHz, resulting in a Rayleigh distance of 26.85 meters.

spired in Fig. 4, the proposed scheme exhibits robust performance in the face of varying distances, whereas the achievable rates obtained by benchmark schemes exhibit marked sensitivity to distance fluctuations. Intriguingly, the performance gap between the proposed scheme and the Perfect CSI benchmark narrows as the distance increases. This indicates that the AI network has the capability to dynamically adjust to environmental variations, allowing the HMIMO codebook to deliver favorable performance not only in the near-field region but also in the conventional far-field scenario.

C. Discussion

This section takes an examination of sampling complexity and pilot overhead of the proposed holographic codebook solution, in comparison to state-of-the-art schemes. Following the philosophy of Type I and Type II codebooks, when sampling over the azimuth-elevation angle pair for an N-element UPA ($N = N_y \times N_z$), $N_y N_z$ sampling points are required for beam training. By contrast, the proposed AI-enabled approach just requires $\tilde{N}$ samples for determining significant angles and $\tilde{U}$ for significant distances for establishing holographic codebook, where $N \gg \tilde{N} + \tilde{U}$.

Regarding pilot overhead, the pilot number for conventional approach (e.g., Type I and Type II) is $\lceil N/N_{\mathrm{RF}} \rceil$. By contrast, our proposed AI-based approach necessitates only a limited number of $P + S$ pilots for the two-phase beam training, where $P = \left\lceil \tilde{N}/N_{\mathrm{RF}} \right\rceil$ and $S = \left\lceil \tilde{U}/N_{\mathrm{RF}} \right\rceil$. Thus, the proposed AI-enabled two-phase approach entails the reduced sampling

TABLE I: Sampling Complexity and Pilot Overhead

	Conventional codebook	Proposed AI-enabled two-phase codebook	
Sampling complexity	$N = N_y \times N_z$	Phase I	$\tilde{N}$
		Phase II	$\tilde{U}$
Pilot overhead	$\lceil N/N_{\text{RF}} \rceil$	Phase I	$P = \left\lceil \tilde{N}/N_{\text{RF}} \right\rceil$
		Phase II	$S = \left\lceil \tilde{U}/N_{\text{RF}} \right\rceil$

complexity and lower occupation of RE resources, despite in the presence of a large number of holographic antenna elements. Table I presents a comparison of the sampling complexity and pilot overhead between the two schemes.

IV. Road to Standardization

We have presented AI-enabled holographic codebook solutions in previous sections. The value of this proposal depends on its future standardization potential for the radio access network (RAN) air interface. Hence, in this section, we delve into the employment of AI in the RAN air interface, in order to envision the evolution of AI-enabled holographic codebooks and their roles in upcoming standard activities. We start by revisiting the concept of the AI-enabled air interface. Then, we enumerate several challenges and present potential impacts on the current standard in the context of HMIMO systems.

A. State-of-the-Art in AI-Enabled Air Interface

Why AI should be utilized for air interface must be a primary concern of wireless communities. Generally speaking, the air interface of an NR RAN consists of numerous interdependent and interconnected modules functioning seamlessly and efficiently with one another. These modules are pragmatically selected in order to decompose an intractable and complex air interface framework into smaller, more tractable functionalities that can be addressed using conventional means. A rapid incorporation of AI techniques into these modules is enhancing RANs functioning within existing standards [13].

Before Release 18, AI-related projects in 3GPP had focused on enabling network automation or data collection for various network functions, such as the network data analytics function introduced in Release 15, which was later improved for data collection and exposure in 5G core in Release 16, and for enabling UE application in Release 17. In Release 17, a RAN-led study on further enhanced data collection investigated the high-level principles of RAN intelligence enabled by AI. This project (included in 3GPP TR 37.817) set out the functional architecture for RAN intelligence and potential benefits of AI-enabled RAN in examination of various use cases [13]. It also led to the approval of a Release 18 normative project on AI for RAN, aiming at guarding its long-term evolution and, potentially, preparing for an AI-endogenous RAN in 6G. Furthermore, the Release-18 RAN1-led study for NR RAN air interface looks into the benefits of enhancing the air interface with the support of AI-based solutions for improved performance at reduced complexity of overhead. The study description has exemplified three promising areas that can be used as a pilot to deepen the understanding of the AI-based solutions, e.g., channel state information (CSI) enhancements, beam management, and direct positioning. These use cases also inspire holographic counterparts in future 6G, such as codebook design empowered by AI.

B. Potential Impact on Standardization

3GPP still has plenty of miles ahead of it in addressing the aforementioned challenges of AI-enabled RAN air interface. In this subsection, we boldly present the potential impact on the standardization within the context of the HMIMO codebook solutions. Fig. 5(a) demonstrates the two-phase signaling procedure between the BS and the UE. Initially, the indices of the antenna elements are predefined at the BS. In Phase I, the UE sends P pilots to the BS for detecting significant angles, with AI functionality at the BS then determining the partial codebook based on these angles. Once Phase I concludes, the UE prepares for the subsequent phase of pilot. In Phase II, the UE sends S pilots, focusing on distances over the earlier identified angles, and the AI functionality is conducted at the BS for the detection of the significant distances.

During each phase, pilot signal configuration encompasses radio resource control (RRC) signaling setup and activation via downlink control information (DCI). These pilots may include sounding reference signals (SRS) or similar uplink reference signals utilized in wireless systems. The '`srs-ResourceSetId`' field can differentiate pilot resources, each tied to specific angular or distance measurements. The '`resourceType`' field categorizes the periodicity of pilot resources (e.g., non-periodic, semi-periodic, or periodic), while the '`usage`' field flags them for channel measurements. For instance, the 'usage' field may adopt values like '`channelMeasurement`', '`beamManagement`', or '`antennaSwitching`'. Additionally, values such as '`channelMeasurement1`' or `channelMeasurement2`' can be introduced to differentiate between angular and distance measurements. The '`SRS-Resource`' field outlines pilot resource sets, while the '`resourceMapping`' field can specify the starting position, symbol count, and repetition factor of the pilot signal resources, among others.

Additionally, the two-phase codebook design dictates that the BS has to configure two types of pilots for the UE at each phase. In addition to specifying the type and the function of SRS, the specific configuration format should include such as the phase index, AI models, and associated parameters. Explicitly, in each phase, the SRS resource sets for angular and distance measurements can be configured and activated via RRC signaling. In each phase, these SRS resource sets can be configured through RRC signaling and activated via the corresponding DCI. For example, the respective SRS resource

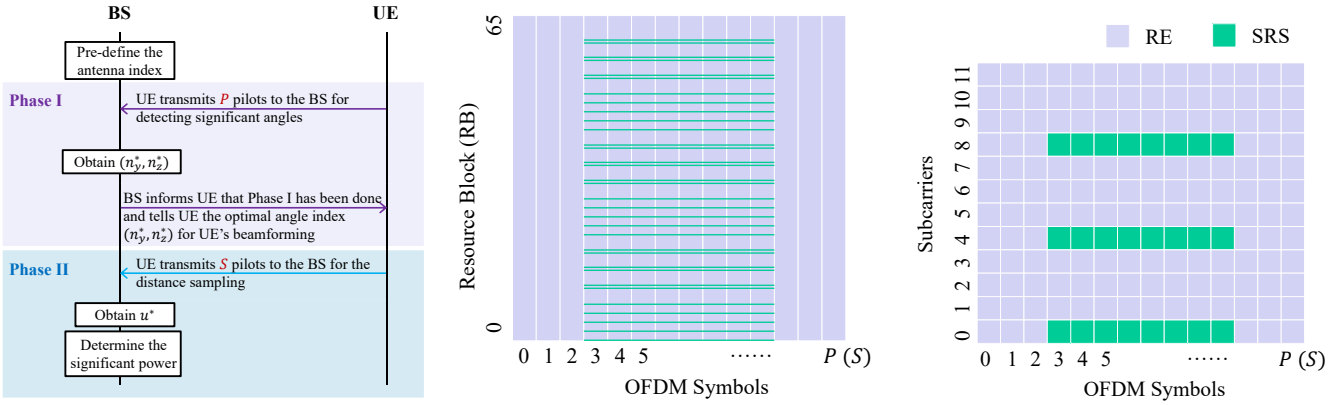

(a) (b) (c)

Fig. 5. (a) Two-phase signaling procedure for HMIMO beam training. (b) Illustration of SRS resource allocation across all resource blocks (RBs). (c) Illustration of SRS occupying resource elements (REs) in a single RB.

sets can be activated by the '`SRS-request`' field in DCI. In another scenario, the aforementioned angle measurement results can be sent to the terminal device in DCI signaling alongside the '`SRS-request`' field. According to TS 38.211 (v17.4.0), the number of SRS symbols can range from 1 to 14, specifically being one of the set $\{1, 2, 4, 8, 10, 12, 14\}$, and the transmission comb number takes values from $\{2, 4, 8\}$ [14]. Hence, in Fig. 5(b) and Fig. 5(c), we illustrate the SRS resource allocation with an example where the transmission comb number is 4 and SRSs occupy 8 OFDM symbols. Fig. 5(b) displays the overall SRS resource occupation across all resource blocks (RBs), while Fig. 5(c) explicitly shows the SRS occupation of REs in a single RB. The pilot pattern can be employed in each phase to carry out angular and distance detection.

V. Conclusion

The evolution of HMIMO technologies adds ever-increasing complexities but brings a host of possibilities for achieving an intelligent and endogenously holography-capable wireless propagation environment. By unveiling the near-field peculiarities in the near-field holographic context, this article proposes a two-phase codebook scheme empowered by AI-enabled approach for efficient beam sweeping. Furthermore, we explore possibilities of ensuring compatibility between the proposal and existing standards, including a two-phase signaling procedure. As 3GPP is ramping up AI projects in standardization evolutions, it is anticipated that AI adoption in air interface will be expedited beyond proprietary solutions, which goes beyond the use of proprietary solutions, with specific attention given to HMIMO as a promising contender for future MIMO technologies.

References

[1] Y. Chen, X. Guo, Z. Wang, and C. Yuen, "Unifying far-field and near-field wireless communications in 6G MIMO," *IEEE Wireless Commun. Lett.*, vol. 13, no. 10, pp. 2762–2766, Oct. 2024.

[2] M. Cui and L. Dai, "Channel estimation for extremely large-scale MIMO: Far-field or near-field?" *IEEE Trans. Commun.*, vol. 70, no. 4, pp. 2663–2677, Apr. 2022.

[3] C. Huang, S. Hu, G. C. Alexandropoulos, A. Zappone, C. Yuen, R. Zhang, M. D. Renzo, and M. Debbah, "Holographic MIMO surfaces for 6G wireless networks: Opportunities, challenges, and trends," *IEEE Wireless Commun.*, vol. 27, no. 5, pp. 118–125, Oct. 2020.

[4] T. Gong, P. Gavriilidis, R. Ji, C. Huang, G. C. Alexandropoulos, L. Wei, Z. Zhang, M. Debbah, H. V. Poor, and C. Yuen, "Holographic MIMO communications: Theoretical foundations, enabling technologies, and future directions," *IEEE Commun. Surveys Tuts.*, vol. 26, no. 1, pp. 196–257, 1st Quart., 2024.

[5] J. An, C. Yuen, C. Huang, M. Debbah, H. Vincent Poor, and L. Hanzo, "A tutorial on holographic MIMO communications—part I: Channel modeling and channel estimation," *IEEE Commun. Lett.*, vol. 27, no. 7, pp. 1664–1668, Jul. 2023.

[6] Y. Chen, X. Guo, G. Zhou, S. Jin, D. W. K. Ng, and Z. Wang, "Unified far-field and near-field in holographic MIMO: A wavenumber-domain perspective," *IEEE Commun. Mag.*, vol. 63, no. 1, pp. 30–36, Jan. 2025.

[7] "Technical specification group radio access network; NR; physical layer procedures for data Release 17," 3rd Generation Partnership Project, Tech. Rep. 3GPP TS 38.214 V17.6.0, Jun. 2023.

[8] Y. Chen, Y. Wang, Z. Wang, and Z. Han, "Angular-distance based channel estimation for holographic MIMO," *IEEE J. Sel. Areas Commun.*, vol. 42, no. 6, pp. 1684–1702, Jun. 2024.

[9] C. Weng, X. Guo, and Y. Wang, "Near-field beam training with hierarchical codebook: Two-stage learning-based approach," *IEEE Trans. Veh. Technol.*, vol. 73, no. 9, pp. 14 003–14 008, Sep. 2024.

[10] Y. Chen, Y. Wang, Z. Wang, and P. Zhang, "Holographic multiple-input, multiple-output systems: Their channel estimation and performance," *IEEE Veh. Technol. Mag.*, vol. 19, no. 3, pp. 48–57, Sep. 2024.

[11] H. Lu and Y. Zeng, "Communicating with extremely large-scale array/surface: Unified modeling and performance analysis," *IEEE Trans. Wireless Commun.*, vol. 21, no. 6, pp. 4039–4053, Jun. 2022.

[12] K. Ma, Z. Wang, W. Tian, S. Chen, and L. Hanzo, "Deep learning for mmwave beam-management: State-of-the-art, opportunities and challenges," *IEEE Wireless Commun.*, to appear, 2022.

[13] X. Lin, "An overview of 5G advanced evolution in 3GPP Release 18," *IEEE Commun. Stand. Mag*, vol. 6, no. 3, pp. 77–83, Sep. 2022.

[14] "Technical specification group radio access network; NR; physical channels and modulation Release 17," 3rd Generation Partnership Project, Tech. Rep. 3GPP TS 38.211 V17.5.0, Jun. 2023.